The Journal of Experimental Biology 204, 2751–2762 (2001)
Printed in Great Britain © The Company of Biologists Limited 2001
JEB3238

HOW THE BODY CONTRIBUTES TO THE WAKE IN UNDULATORY FISH SWIMMING: FLOW FIELDS OF A SWIMMING EEL (*ANGUILLA ANGUILLA*)

ULRIKE K. MÜLLER*, JORIS SMIT, EIZE J. STAMHUIS AND JOHN J. VIDELER

Department of Marine Biology, University of Groningen, PO Box 14, 9750 AA Haren (Gn), The Netherlands

*Present address and address for correspondence: Department of Zoology, University of Cambridge, Downing Street, Cambridge CB2 3EJ, UK (e-mail: ukm20@cam.ac.uk)

Accepted 31 May 2001

Summary

Undulatory swimmers generate thrust by passing a transverse wave down their body. Thrust is generated not just at the tail, but also to a varying degree by the body, depending on the fish's morphology and swimming movements. To examine the mechanisms by which the body in particular contributes to thrust production, we chose eels, which have no pronounced tail fin and hence are thought to generate all their thrust with their body. We investigated the interaction between body movements and the flow around swimming eels using two-dimensional particle image velocimetry. Maximum flow velocities adjacent to the eel's body increase almost linearly from head to tail, suggesting that eels generate thrust continuously along their body. The wake behind eels swimming at 1.5 L s^{-1}, where L is body length, consisted of a double row of double vortices with little backward momentum. The eel sheds two vortices per half tail-beat, which can be identified by their shedding dynamics as a start–stop vortex of the tail and a vortex shed when the body-generated flows reach the 'trailing edge' and cause separation. Two consecutively shed ipsilateral body and tail vortices combine to form a vortex pair that moves away from the mean path of motion. This wake shape resembles flow patterns described previously for a propulsive mode in which neither swimming efficiency nor thrust is maximised but sideways forces are high. This swimming mode is suited to high manoeuvrability. Earlier recordings show that eels also generate a wake reflective of maximum swimming efficiency. The combined findings suggest that eels can modify their body wave to generate wakes that reflect their propulsive mode.

Key words: fish, swimming, undulatory swimming, eel, *Anguilla anguilla*, flow visualisation, particle image velocimetry.

Introduction

Many fish pass a transverse wave down their body to produce thrust. Undulatory swimming comprises a continuum of swimming styles from curvilinearly increasing body waves running down fusiform bodies and generating thrust mainly at the tail to rectilinearly increasing body waves along elongate bodies generating thrust along the whole body. At one end of the spectrum are fish such as mullet *Chelon labrosus* (Müller et al., 1997) and danio *Danio malabaricus* (Wolfgang et al., 1999), both with a curvilinearly increasing amplitude envelope and thrust production dominated by the contribution of the tail. Two mechanisms have been proposed to explain how the body contributes to the thrust generated at the tail. First, the body undulations create circular flow patterns that travel posteriorly along with the body wave and ultimately modify the flow around the tail to increase swimming performance (Müller et al., 1997). The second mechanism is based on shedding vorticity off the body's trailing edge in the peduncle region, which again modifies the tail flow to increase swimming efficiency (Wolfgang et al., 1999). Eels (*Anguilla anguilla*), with their elongate bodies and rectilinearly increasing body wave, represent an extreme case of undulatory swimming and generate thrust along their whole body rather than at the tail. A snapshot of the flow around and behind their body has been published (Gray, 1968) and resembles the flow patterns observed in mullet and danio. But, without a description of the eel's swimming kinematics, no link between body movement and flow can be established. It is, however, unlikely that the trailing edge shedding mechanism contributes to thrust since eels do not have a peduncle region and body vorticity cannot be shed in this way to interact with the tail flow.

Simple analytical models predict that undulatory swimmers shed a reverse von Kármán vortex street when optimising swimming performance (Lighthill, 1969). This wake consists of a double row of single vortices and is generated if the fish swims at a slip (the ratio of swimming speed U to body wave speed V) of less than 1. Typically, slip is in the region of 0.6–0.8 (for a review, see Videler, 1993). Computational simulations of the flow around an undulatory swimmer exist for a danio (Wolfgang et al., 1999) and eel (Carling et al., 1998; Pedley and Hill, 1999). Two of the three models predict a wake resembling the prediction of Lighthill (Lighthill, 1969) with

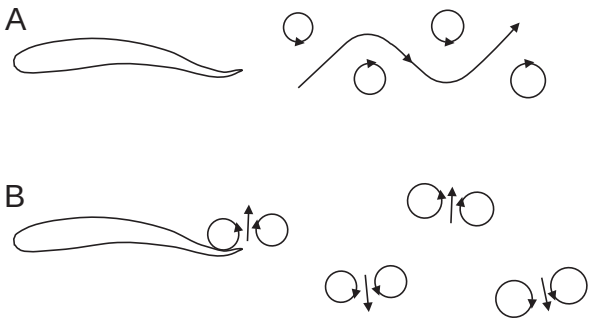

Fig. 1. Sketch of a cross section in the medio-frontal plane of the wake behind a steady undulatory swimmer. (A) Double row of single vortices as observed in eel, bream, trout and mullet, which in three dimensions constitute a chain of vortex rings (Blickhan et al., 1992). (B) Double row of double vortices as observed in zebra danio, water snake and Kuhli leach. The circles indicate shed vortices, with arrowheads indicating the rotational sense. The arrows indicate the jet flows.

one vortex shed per half tail-beat. Carling et al. (Carling et al., 1998) predict a wake consisting of two counter-rotating vortices on either side of the mean path of motion, into which all shed vortices merge. However, model studies on waving plates have shown that the wake changes significantly with slip (Hertel, 1966) and the phase between interacting waving plates (Gopalkrishnan et al., 1994; Streitlien et al., 1996).

The experimental flow fields published so far have concentrated on the wake rather than on wake generation. Two main wake patterns have been observed behind undulatory swimmers (Fig. 1). The reverse von Kármán vortex street, indicative of high efficiency, has been observed in eel (Gray, 1968), bream *Diplodus annularis* (Aleyev, 1977), trout *Oncorhynchus mykiss* (Blickhan et al., 1992) and mullet (Müller et al., 1997). A different vortex pattern resembling a double row of double vortices has been reported for zebra danio *Brachydanio albolineatus* (Rosen, 1959), water snake *Natrix natrix* (Hertel, 1966) and Kuhli leach *Acanthophthalmus kuhli* (Rayner, 1995). All these wake patterns were generated during steady undulatory swimming at speeds between 1 and $7\,L\,s^{-1}$, where L is body length. The values for slip were 0.6–0.7 where mentioned.

In the present study, we address the question of how a wake is generated by the interaction between fish and water. Quantitative mapping of the flow, from its generation on the body to the shedding of the wake, will provide a time course of wake development. If thrust is generated along the whole body, flow speeds adjacent to the body should increase continuously from head to tail, rather than increase sharply towards the tail as observed in carangiform swimmers (Müller et al., 1997; Wolfgang et al., 1999). Mapping swimming movements and flow simultaneously will suggest the relevant kinematic parameters for thrust production. Key wave parameters such as maximum lateral displacement and lateral velocity will be mapped relative to the flow to establish correlations between body wave and flow. Previous work has shown that eels generate flow fields around their body and in their wake that are qualitatively equivalent to the flow fields of carangiform swimmers such as mullet and danio. The eel is also the most extreme case of body-generated thrust: without a pronounced tail, an eel generates thrust along the whole of its body. Hence, eels provide the ideal showcase for thrust-generating mechanisms of the body during steady undulatory swimming.

Materials and methods

Experimental animals

The experiments were performed on juvenile eels *Anguilla anguilla* L. caught as glass-eels during the winters of 1995/96 and 1996/97 off the Portuguese coast and kept for 3 months at an eel farm in the Netherlands. They were reared to the elver stage in a 30 l aquarium containing artificial sea water (salinity 30 ‰) at 22±1 °C. At the time of the experiments, the eels were approximately 0.10 m in body length L and less than 5 mm high.

Flow visualisation

The experiments were performed in still-standing water. This allows the eel to display its preferred swimming behaviours spontaneously. In still-standing water, the signal-to-noise ratio in the flow visualisation is maximal in the absence of turbulence induced by the flow tank. The eels swam in a 0.2 m×0.3 m×0.3 m tank filled to a depth of at least 50 mm with artificial sea water (salinity 30 ‰, temperature 22 °C). The water was seeded with unexpanded polystyrene particles (VF 654, BASF, diameter 0.2–0.4 mm). The particles were slightly denser ($1.026\,kg\,m^{-3}$) than sea water, so their response to changes in the flow velocity was delayed (Merzkirch, 1987) and they sank slowly. Both effects were insignificant compared with the fish-generated flows and were therefore neglected. The particles were illuminated in a horizontal plane by a 1 mm thin laser light sheet (krypton ion laser, wavelength λ=647 nm, maximum power 0.8 W). A horizontal light sheet was positioned in the middle of the water column. The water surface was covered with a Plexiglas raft to prevent surface waves from distorting the images when the fish was swimming too close to the water surface. We recorded sequences only when the fish was swimming in the middle of the tank to avoid wall and surface effects. Only spontaneous swimming behaviour was recorded; we did not stimulate the fish in any way.

All experiments were performed with a single fish in the test tank. The fish avoided looking into the light sheet by keeping its eyes above or below the level of the light sheet. Otherwise, swimming behaviour seemed to be unaffected by the light sheet. A CCD camera (Adimec MX-12, with 50 mm lens and 5 mm extension ring) was mounted perpendicular to the light sheet to record top-view images of 1024×1024 pixels at a frequency of $25\,images\,s^{-1}$ (integration time 10 ms). Recordings of the flow fields were made using a purpose-designed recording system (Dutch Vision Systems) (Müller et

al., 1997). The recorded images were checked immediately, and sequences in which the eel and the wake were in the light sheet in the centre of the field of view were stored uncompressed as 512×512 pixel images for later analysis. We filmed in the centre of the tank to avoid recordings impaired by wall effects. We recorded up to five sequences from 11 eels.

Kinematic analysis

In the selected sequences, the eel was swimming horizontally through the light sheet along a straight path through the centre of the field of view, i.e. with its body at least 25 mm away from the water surface and the bottom of the tank. We obtained the midlines of the swimming eel from the digitised images (TIM, Dutch Vision Systems) (Müller et al., 1997). The body length was assumed to be equivalent to the number of pixels representing the midline of the fish. The instantaneous swimming speed was obtained from the head position in sequential images and the frame rate. It was averaged over complete tail-beat cycles to obtain the mean swimming speed U. The mean path of motion was calculated from the head position in consecutive images using standard linear regression over complete tail-beat cycles.

In an earth-bound frame of reference, we calculated the following kinematic parameters. The amplitude A of the body wave at each point along the body was defined as half the transverse distance between the points of maximum lateral excursion of a particular body segment. The stride length λ_s of the fish was calculated as twice the distance between two consecutive points where the path of the tail crosses the mean path of motion. We also determined the lateral velocity $V(t,x)$ of the body relative to the fluid and the points on the midline where this lateral velocity is zero [for a definition of $V(t,x)$, see Appendix].

The following kinematic parameters were obtained in a fish-bound frame of reference. The body wave length λ_b was considered to be twice the distance between two consecutive points where the body midline crosses the mean path of motion. The speed V of wave propagation was calculated from the displacement of these crossings and the frame rate (25 Hz). We further determined the position of the nodes, maxima and inflection points of the midline. The nodes were defined as the points where the midline crosses the mean path of motion. The inflection points were defined as the points where the curvature of the midline changes direction. Nodes, maxima and inflection points of the midline were derived numerically by searching for zero positions and extremes in the lateral displacement function and its derivatives (Müller et al., 1997).

Hydrodynamic analysis

Particle image velocimetry

The flow generated by the swimming fish was visualised using two-dimensional particle image velocimetry (PIV). The exact algorithms employed to derive the flow fields from our recordings are described elsewhere (Stamhuis and Videler, 1995).

We conducted subimage cross-correlations on pairs of consecutive images to obtain a velocity vector field from the particle displacements (Chen et al., 1993; Stamhuis and Videler, 1995). We used a subimage size of 33×33 pixels with 50 % overlap. The choice of the subimage size was determined by the seeding density of the polystyrene particles and the peak velocities in the flow fields (Keane and Adrian, 1991): there were more than 10 particles in each subimage; the particle displacement in the flow was less than 25 % of the subimage diameter between consecutive frames. The cross-correlation resulted in vector fields of, at best, 30×30 equally spaced vectors if all subimages contained sufficient information for cross-correlation. A comparison of particle tracking results with PIV flow velocity data for the same area in the flow field revealed no significant underestimation of the peak flow velocities due to the spatial averaging of the cross-correlation. Regions in which PIV was not possible or was unreliable were augmented by particle tracking velocimetry (as described in Müller et al., 1997).

Post-processing

The flow velocity vectors resulting from PIV were fitted into a grid of 30×30 cells. Gaps in the resulting vector field were filled using a two-dimensional spline to interpolate vectors (Stamhuis and Videler, 1995). The following flow parameters were derived from the flow field: vorticity ω, which is proportional to the angular velocity at a point in the fluid, and the discriminant for complex eigenvalues d, which was used to locate the centre of vortices in the wake (Vollmers et al., 1983; Stamhuis and Videler, 1995).

The wake was characterised by the position of the vortex centres and the direction of the jet. From the position of the vortex centres in the flow field, we calculated the distance between vortices along and perpendicular to the mean path of motion. Consecutive vortices were considered to be a pair and, hence, were assumed to form a vortex ring in the three-dimensional wake if they were separated by a distinct jet flow and moved away from the mean path of motion together. We also confirmed that their respective circulations were equal in magnitude and of opposite sense after shedding. The forward momentum that the fish is able to gain from such a vortex ring depends on the momentum angle φ between the ring and the mean path of motion. The angle between the ring and the mean path of motion and the flow speed of the jet through the ring were obtained directly from the velocity vector field.

All mean values in the text are given ± 1 S.D.

Results

We recorded 30 sequences, each of approximately three tail-beats, in which the eel was swimming in the field of view at swimming speeds between 0.10 and 0.15 m s^{-1}. In half of these, the eel shed a structured wake always consisting of one vortex pair per tail-beat. We did not succeed in recording a single sequence in which the eel reproduced the wake pattern photographed by Gray (Gray, 1968). Of the recorded sequences, three were selected for further analysis on the basis

Table 1. *Morphological and kinematic parameters for the three swimming sequences selected for analysis*

		Sequence		
		1 (Fig. 2A)	2 (Fig. 2B)	3 (Fig. 2C)
Body length, L	m	0.08	0.10	0.10
Swimming speed, U	m s^{-1}	0.12	0.14	0.10
Wave speed, V	m s^{-1}	0.21	0.20	0.15
Tail-beat frequency, f	s^{-1}	2.6	2.3	2.8
Tail-beat amplitude, A	m	0.09	0.10	0.10
Stride length, λ_s	L	0.5	0.6	0.4
Body wave length, λ_b	L	0.87	0.69	0.85
Slip, U/V		0.6	0.7	0.7

of their high and even seeding with the eel swimming horizontally in the light sheet without noticeable changes in direction or speed. Their wakes consisted of a double row of double vortices. The fish swam in the centre of the field of view in only one of the chosen sequences. All but two flow fields presented stem from this one sequence to facilitate comparison amongst the figures.

Swimming kinematics

In the selected three sequences (Fig. 2), the eels have similar tail-beat frequencies, amplitudes and body wave lengths (Table 1). They cross the field of view within three tail-beat cycles. Their slip U/V ranges from 0.6 to 0.7 at swimming speeds of 0.10–0.14 m s^{-1} (1.0–1.5 L s^{-1}). Within one tail-beat cycle, the swimming speed varies between 0.9 and 1.1U. Swimming speed exhibits a total of two peaks per half tail-beat cycle, with both peaks clustering around the moment of stroke reversal of the tail. The kinematic characteristics of the undulating body movements agree with earlier findings (Hess, 1983; Videler, 1993). The amplitude envelope of the body wave shows a minimum at a distance 0.1L from the snout tip and increases from there almost linearly to a maximum amplitude of approximately 0.1L at the tail tip. The body wave length decreases along the body by 20–30 % from above 1.0L in the first third of the body to 0.8L at the tail. The stride length λ_s is approximately 0.5L.

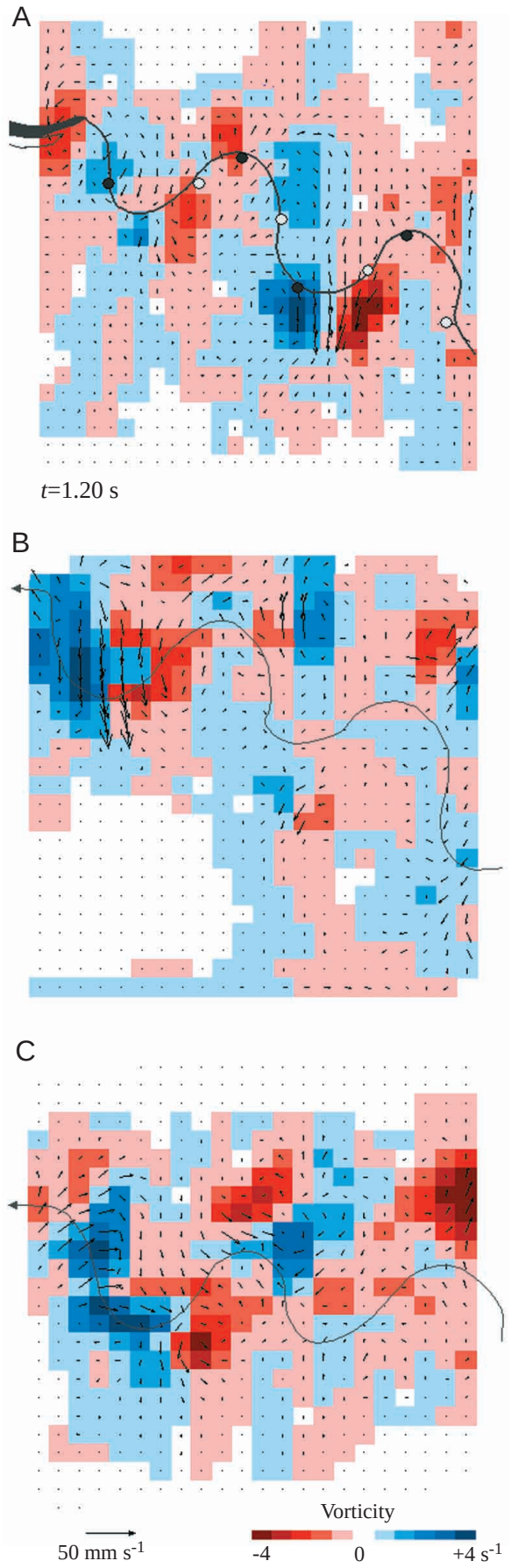

Fig. 2. The wake behind a steadily swimming eel. The short black arrows indicate the flow velocity. The meandering grey arrow indicates the path of the tail tip and the swimming direction. All eels are swimming from right to left and have just left the field of view. The colour tiles indicate the level of vorticity in the flow, blue for clockwise vorticity, red for counterclockwise vorticity. Darker shades indicate higher levels of vorticity. The field of view is 108 mm×108 mm. (A) Eel (body length L=0.08 m) swimming at speed U=0.12 m s^{-1}. Sequence 1, see Table 1. Tail and body vortices have moved away from their initial shedding position (filled and open circles, respectively) close to the tail path (grey line). The shed vortices are visible in the flow field as areas of elevated vorticity. (B) Eel (L=0.10 m) swimming at U=0.14 m s^{-1}. Sequence 2, see Table 1. (C) Eel (L=0.10 m) swimming at U=0.12 m s^{-1}. Sequence 3, see Table 1.

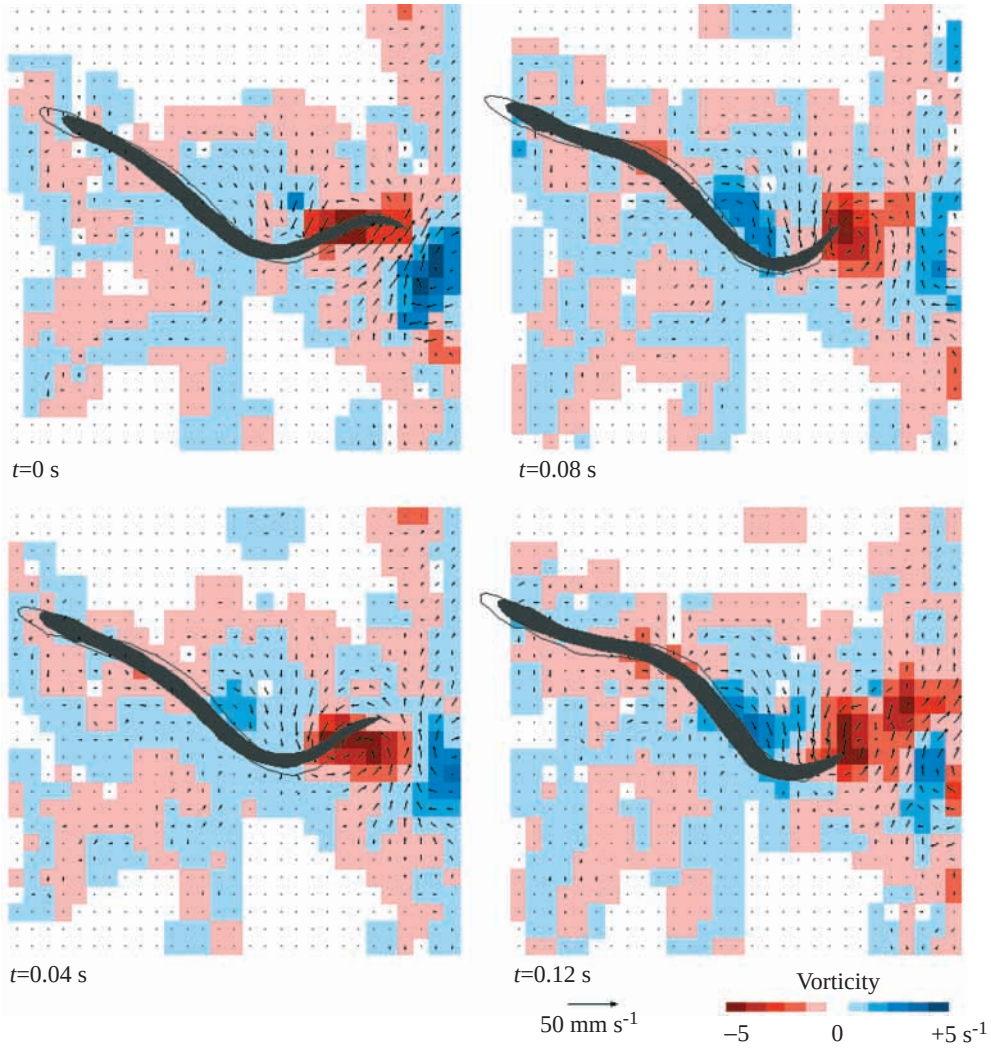

Fig. 3. Flow field adjacent to an eel (body length L=0.079 m) swimming steadily at speed U=0.121 m s^{-1} from the lower right to the upper left of the field of view (sequence 1, see Table 1). The black arrows indicate the flow velocity. Blue shades indicate clockwise vorticity, red shades indicate counterclockwise vorticity. Darker shades indicate higher levels of vorticity. The flow fields are continued in Fig. 6. The time t is arbitrarily set to t=0 s for the first frame shown in Fig. 3. The field of view is 108 mm×108 mm.

Flow in the vicinity of the fish body

Flow generated by the body

A swimming eel generates substantial flows from the crests to the troughs of the body wave along the full length of its body (Fig. 3). In the medio-frontal plane of the body, these flows form semicircles that travel posteriorly with the body wave. In a fluid-based reference system, the flows from crests to posterior troughs are strong, unlike the flows from crests to anterior troughs. As the body wave amplitude increases posteriorly, so do the flows. The peak flow speeds in the crests increase almost linearly from values close to 0 directly behind the head to 0.014 m s^{-1} (0.12U) at the tail (Fig. 4). In the troughs, the flow speeds increase to values of up to 0.023 m s^{-1} (0.19U) at the tail. Contralateral semicircular flows have the same sense of rotation. Combined, they resemble the potential region of a vortex that has its centre within the eel's body, their flow driven by the pressure difference between crests and troughs. With each high-pressure flow off a crest being followed by a low-pressure flow into the neighbouring trough, the maximum size of this vortical structure is limited to a quarter of the body wave length. The 'vortex' centre is located

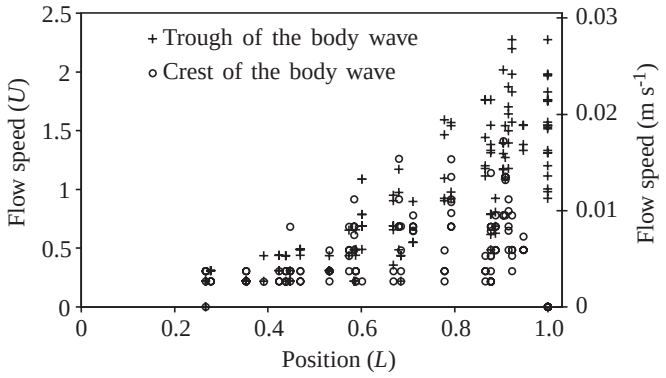

Fig. 4. Variation in the flow speeds adjacent to the eel's body over one tail-beat cycle. The values at a particular position along the body can range from close to zero when the body segment is close to an inflection point of the midline to maximum values when the segment is in the low- or high-pressure zone. The maximum flow speeds, indicative of the transferred momentum, increase almost linearly from head to tail.

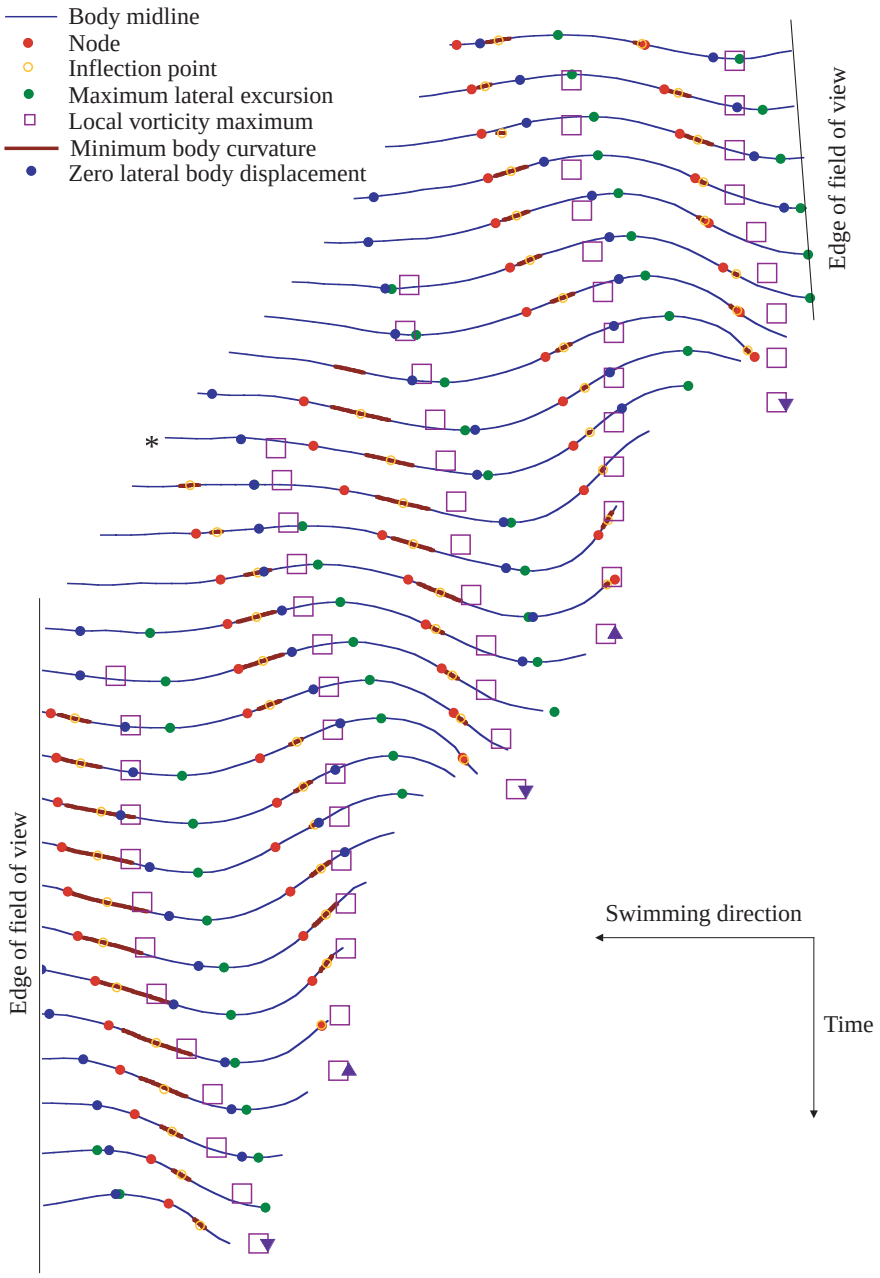

Fig. 5. Midlines of a steadily swimming eel over approximately two tail-beat cycles in an earth-bound frame of reference (swimming speed U=0.121 m s^{-1}, sequence 1, see Table 1; see also Fig. 2A, Fig. 3 and Fig. 6 for flow fields). Also shown are the positions of several body wave parameters and the location of maximum vorticity in the flow field. The time interval between consecutive midlines is 0.04 s. The vertical lines at either side of the graph indicate the edge of the recorded images. The asterisk indicates t=0 s (cf. Fig. 3 and Fig. 6). The purple boxes indicate the grid cells with a local maximum in vorticity, sized to scale. Their arrowheads indicate the sense of rotation of the shed vortex. The area of minimum curvature (brown bar) indicates the confidence interval of the location of the inflection point.

between the crest and the trough of the body wave in the regions of elevated vorticity adjacent to the eel's body. This vortical flow travels down the body along with the body wave and is ultimately shed in the wake as a vortex. While still travelling along the body, we call this structure a 'proto-vortex'. Once it has been shed, it is called a 'body vortex'. The term 'bound vortex' is avoided because our experimental evidence does not show conclusively that the observed phenomenon is a vortex or that it is in any way equivalent to a 'bound vortex', which is a free vortex core 'buried' inside a lift-generating aerofoil to satisfy the Kutta–Joukowsky theorem.

Blickhan et al. (Blickhan et al., 1992) and Videler et al. (Videler et al., 1999) suggest that the undulatory pump mechanism is driven by a combination of a travelling wave with a posteriorly increasing amplitude envelope. The centre of the 'proto-vortex' is therefore correlated with the transition point between concave and convex body curvature. Triantafyllou et al. (Triantafyllou et al., 2000) find in their computational flow fields that local peaks in the boundary layer vorticity occur near the nodes of the body wave. To test these proposed links between body kinematics and flow, the position of the vortex centre was tested against the position of the following three body wave parameters: (i) the node, where the body midline crosses the mean path of motion; (ii) the maximum, where the body wave reaches local extremes of lateral excursion; and (iii) the inflection points, where the direction of the body curvature changes. The centre of the

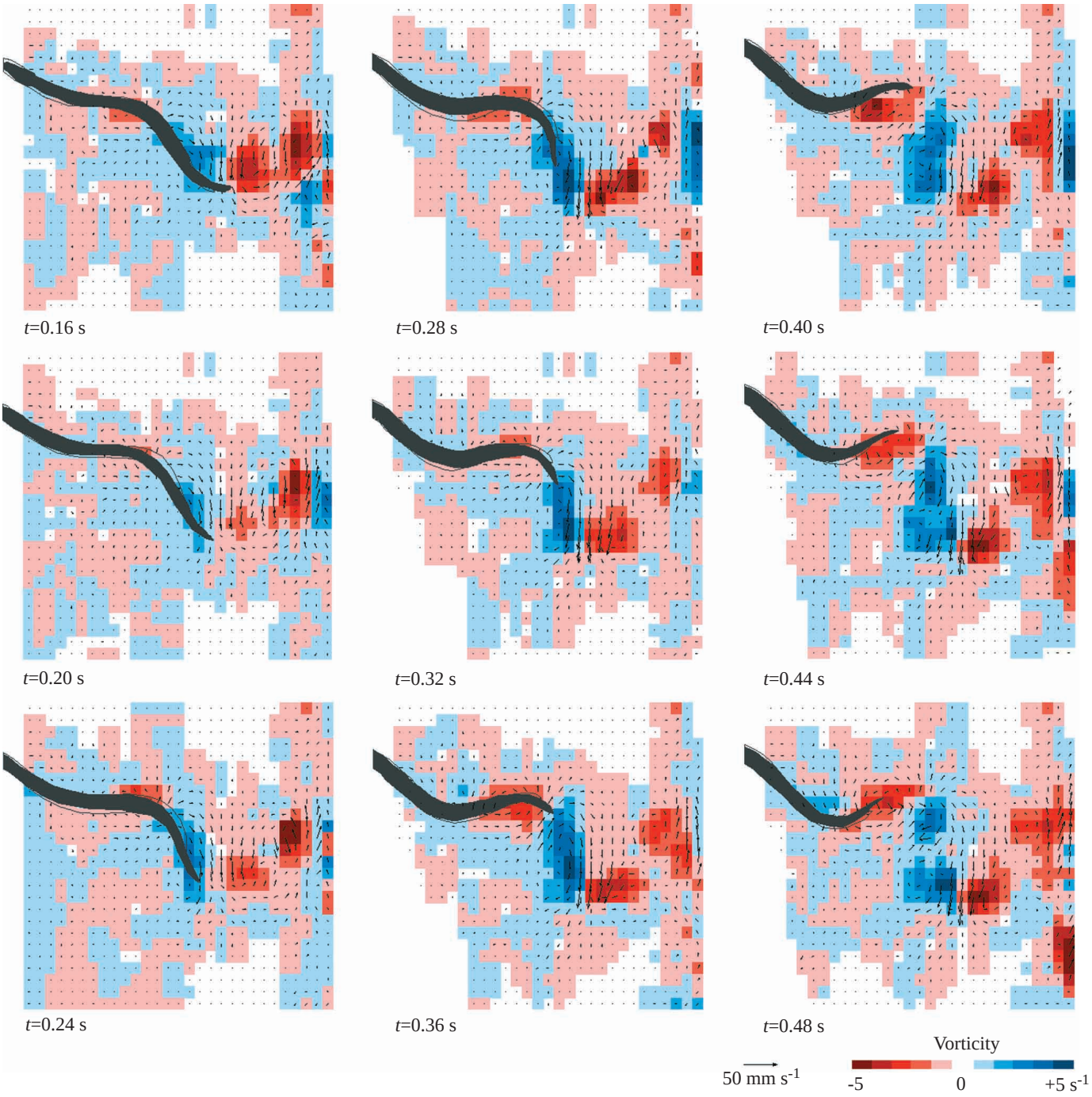

Fig. 6. Instances during the time course of wake generation behind a steadily swimming eel (speed U=0.121 m s^{-1}, sequence 1, see Table 1). The black arrows indicate the flow velocity, and the colour code indicates vorticity. Blue shades indicate clockwise vorticity, red shades indicate counterclockwise vorticity. Darker shades indicate higher levels of vorticity. The flow fields are a continuation of the swimming sequence in Fig. 3. The time t is arbitrarily set to t=0 s for the first frame shown in Fig. 3. The field of view is 108 mm×108 mm.

'proto-vortex' was assumed to be at the local vorticity peak. We found that, within the limited spatial resolution of our flow fields (3 mm), none of the above body wave parameters correlates tightly with the position of the vortex centre. Instead, the vortex centre shifts from a position close to the lateral maximum when near the head until it almost coincides with the position of the node and inflection point when it is shed off the tail (Fig. 5, Fig. 6). The phase between node and vortex centre induces a lateral offset that decreases with decreasing phase. Ultimately, the 'proto-vortex' crosses the mean path of motion together with the inflection point and is shed off the tail on the opposite side (Fig. 6, t=0.48 s; t=0 s is defined in Fig. 3) from where the vortex was first observed at approximately 0.3L behind the head (Fig. 3, t=0.04 s).

To test whether the observed vorticity distribution is consistent with a simple lift generation model (Lighthill's slender body model: Lighthill, 1960), we also calculated the lateral velocity $V(t,x)$ of the body relative to the fluid. A body of constant cross-sectional area A swimming in water of density ρ creates instantaneous lift forces F_L at each body segment according to:

$$F_L = -\rho A V(t,x)\,. \quad (1)$$

At the centre of the 'proto-vortex', $V(t,x)$ should be zero. The precision of zero positions of $V(t,x)$ decreases anteriorly from less than 1 mm at the tail to 10 mm near the head. Within these limits, the points along the midline where $V(t,x)$ is zero coincide with the positions of local vorticity maxima only for the counterclockwise vortices. For the clockwise vortices, there is a variable phase shift between the two. These tentative results, together with predictions of an analytical body wave model (see Appendix), suggest that body wave parameters are not suitable for predicting the body flows directly. In the present study, a simple two-dimensional pressure-based model yields more reliable predictions, but its power is limited because it ignores three-dimensional effects and wake interaction.

Flow generated at the tail

The flow at the tail results from the interaction between the body flow reaching the tail and the flow generated by the oscillating movement of the tail. Over most of the tail-beat cycle, it has a strong lateral component. This is mainly a result of the body-generated low-pressure flows periodically entering the tail region. Averaged over one tail excursion from right to left, flow velocities are 0.019±0.004 m s^{-1} (0.16±0.03U) (N=23 velocity vectors from t=0.08 s in Fig. 3 to t=0.24 s in Fig. 6). Flow velocities in the grid cells adjacent to the tail vary over half a tail-beat cycle from 0.014±0.006 m s^{-1} (0.12±0.05U) (N=27 velocity vectors from three tail-beats from t=0 s in Fig. 3 to t=0.64 s in Fig. 6) when the tail crosses the mean path of motion to 0.021±0.008 m s^{-1} (0.18±0.07U) (N=14 velocity vectors from three tail-beats) near the stroke reversal. The peak velocities coincide with the body flows entering the tail region. At this moment, the mean angle of attack of the tail (the angle between the flow and the tail fin) is approximately 50 ° (49±5 °, N=3 tail-beats), and a vortex is shed off the tail (Fig. 3, t=0.12 s; Fig. 6, t=0.32 s). Body vortices shed to the right of the animal just before stroke reversal rotate clockwise; body vortices shed to the left rotate counterclockwise.

Each time the tail reaches a lateral extreme and changes direction, a start–stop vortex is shed at the tip of the tail. This vortex is visible in the wake as a circulating flow around an area of elevated vorticity (e.g. Fig. 6, t=0.24 s and 0.44 s). Tail vortices shed to the right of the animal rotate counterclockwise (Fig. 6, t=0.44 s); vortices shed to the left of the animal rotate in a clockwise direction (Fig. 6, t=0.24 s). In the following, start–stop vortices shed at stroke-reversal from the trailing edge of the tail will be called tail vortices. Because of the limited spatial resolution of our flow fields, a body vortex is not always distinguishable from the previously shed tail vortex during and immediately after shedding (Fig. 6, t=0.24–0.36 s). However, both emerge as separate and individually recognisable body and tail vortices in the wake by the time the next body vortex is shed (Fig. 6, t=0.40 s).

Flow in the wake

Wake morphology and wake generation

In all sequences with a clearly visible wake, the flow field in the medio-frontal plane behind a swimming eel consists of four vortices per tail-beat cycle (Fig. 5, Fig. 6). Consecutively shed ipsilateral vortices have an opposite sense of rotation. This induces a strong jet flow between them. The jet has only a small component in the direction opposite to the swimming direction, but is directed away from the mean path of motion at almost a right angle (φ=70±10 °, N=3 tail-beats from t=0 s in Fig. 3 to t=0.64 s in Fig. 6). This suggests that the eel is generating considerable side forces and little thrust. The flow speeds of the jet are 0.016±0.005 m s^{-1} (0.13±0.05U; N=3 tail-beats). The vortices move away from the mean path of motion, and the distance between the contralateral vortices roughly doubles within 0.5 s.

A pattern of double vortices in a double row could be a cross section through either of the proposed wakes (Fig. 1). First, if the wake behind the fish is a single chain of vortex rings (Fig. 1A, Fig. 7A), a frontal cross section of such a vortex chain off the medial plane would consist of two rows of vortex pairs. Two consecutive ipsilateral vortices would have the same rotational sense. The jet through the centre of the vortex rings would appear to meander between consecutive counter-

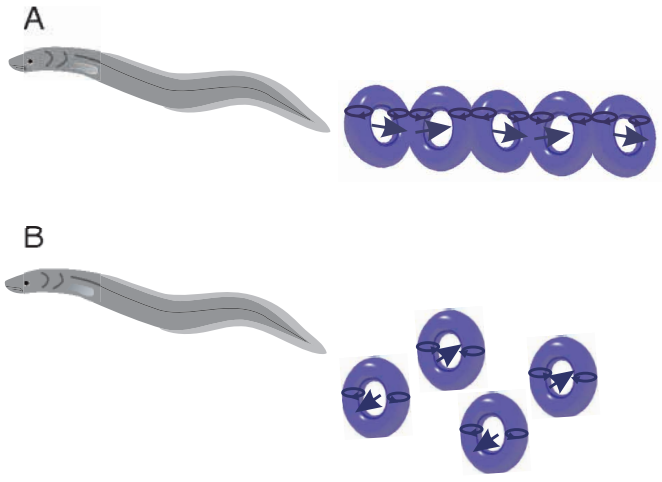

Fig. 7. Hypothetical three-dimensional wakes of an eel. (A) In a cross-sectional view above or below the medio-frontal plane, a single vortex chain would appear as pairs of same-sense vortex pairs to either side of the mean path of motion. A strong jet flow meandering around the mean path of motion would be visible between consecutive contralateral vortices. (B) A double vortex ring wake viewed in the mediofrontal plane would appear as pairs of counter-rotating vortices to either side of the mean path of motion. A jet flow would form between the vortices of a pair. Our two-dimensional flow fields are consistent with scenario B rather than A.

rotating vortices on opposite sides of the mean path of motion. Second, two ipsilateral counter-rotating vortices could be a mediofrontal cross section through a vortex ring with a jet through the centre of the ring. The three-dimensional impression of such a wake would be a double row of vortex rings (Fig. 1B, Fig. 7B). These individual vortex rings would move away from the mean path of motion at their self-induced velocity.

In our flow fields, consecutive ipsilateral vortices are counter-rotating. The distance between contralateral vortices perpendicular to the mean path of motion increases over time, while the distance along the mean path of motion remains constant. On the basis of these observations, we assume that consecutive ipsilateral vortices represent cross sections through a vortex ring with a diameter that can be approximated by the distance between the two vortices (Fig. 7B).

One vortex ring comprises consecutively shed ipsilateral body and tail vortices. A clockwise tail vortex combines with the previously shed counterclockwise body vortex to form a vortex ring to the left of the mean path of motion, and *vice versa* for vortex rings to the right of the mean path of motion. Body and tail vortices can be distinguished by their position relative to the path of the tail tip (Fig. 2A). Tail vortices are shed just after the point of maximum lateral displacement of the tail, and body vortices are shed before this point close to the mean path of motion. The positions of the vortices reflect the swimming kinematics. The distance between the centres of consecutive tail vortices and between consecutive body vortices along the mean path of motion is 22±4 mm (N=3 tail-beats from t=0 s in Fig. 3 to t=0.64 s in Fig. 6), which matches half the stride length λ_s (λ_s=46±5 mm, N=3 tail-beats). Vortices of the same type do not move apart along the mean path of motion during the observation period of 1 s. The initial distance between shedding positions of consecutive tail vortices perpendicular to the path of motion is 20.1±4.3 mm (N=3 tail-beats). This corresponds to twice the tail-beat amplitude A (A=9.3±1.0 mm, N=3 tail-beats). The distance between consecutive contralateral tail vortices almost doubles during the first second after shedding. The body vortices move apart perpendicular to the mean path of motion at the same rate. However, at 2.6±2.1 mm (N=3 tail-beats), the initial distance between consecutive contralateral body vortices is considerably smaller than twice the tail-beat amplitude and is closer to the distance between consecutive inflection points as they reach the tail tip (4.4±3.2 mm, N=3 tail-beats).

If the circulation Γ and radius R of a circular vortex ring are known, the vortex ring impulse I can be computed according to (Spedding et al., 1984):

$$I = \rho\Gamma\pi R^2 . \quad (2)$$

Immediately after shedding, body and tail vortices have a similar strength, which varies between rings from 0.0003 to 0.0007 $m^2 s^{-1}$. This circulation is equivalent to a vortex force of 0.4–1 mN. At a momentum angle of 70 °, this corresponds to a net thrust of 0.1–0.3 mN.

Discussion

Contribution of the body to the wake in undulatory swimmers

Lighthill (Lighthill, 1969) predicted that the body would generate thrust at slips smaller than unity by imparting rearward momentum to the fluid. On the basis of their own flow visualisations, Rayner (Rayner, 1985) and Blickhan et al. (Blickhan et al., 1992) also proposed that the body would contribute to thrust production. Rayner called the flow patterns generated on the body ‘trapped vortices’ (Rayner, 1985). Blickhan et al. (Blickhan et al., 1992) coined the phrase ‘undulatory pump’ to describe thrust production by body undulation. Both base their concepts on observations of undulatory swimmers generating considerable potential flows along their body. Lighthill’s (Lighthill, 1969) analytical model predicts that fish will shed only a single vortex street, whereas in our study body and tail flows are shed at separate instances into a double vortex street. This wake pattern was anticipated in model experiments and computational studies (Gopalkrishnan et al., 1994; Streitlien et al., 1996). According to their findings, at least three types of vortex interaction can be anticipated. One possible scenario maximises thrust and results in the shedding of a single reverse von Kármán vortex street, because body and tail vortices of the same rotational sense are shed together and merge. Another scenario maximises efficiency, and a single weak von Kármán vortex street results from the merging of counter-rotating tail and body vortices into one shed vortex per half tail-beat. A third scenario emerges from counter-rotating body and tail vortices being shed at discrete instances. The resulting wake behind the fish contains two vortex pairs per tail-beat cycle. While Triantafyllou et al. (Triantafyllou et al., 2000) emphasise the role of body vorticity shed at the caudal peduncle in modifying the propulsive performance of the tail, we would like to propose a modified model of wake generation for undulatory swimmers. This model does not require trailing-edge shedding off the body and is, therefore, also applicable to elongate swimmers such as the eel without a peduncle region or discrete dorsal fins.

At slips smaller than unity, the swimmer transfers momentum when the lateral movements of its body accelerate the adjacent water. This generates longitudinal flows that are driven by the pressure gradient between ipsilateral troughs and crests of the body wave. With the body wave amplitude increasing towards the tail, this momentum transfer takes place along the entire body; as the body wave amplitude increases, so do the longitudinal flows. The localised pressure gradients not only cause flows from body wave crests to posterior troughs, but also cause a backflow from high-pressure to anterior low-pressure zones. This backflow, in turn, causes a thickening of the boundary layer in a region along the body approximately at the core of the ‘proto-vortex’. This thickening effect becomes visible only in slender swimmers, for which the flows are stronger than in fusiform swimmers; in these areas of backflow, the boundary layer occupies a large enough proportion of a grid cell to elevate its average vorticity significantly.

Computational studies on fusiform swimmers (Triantafyllou

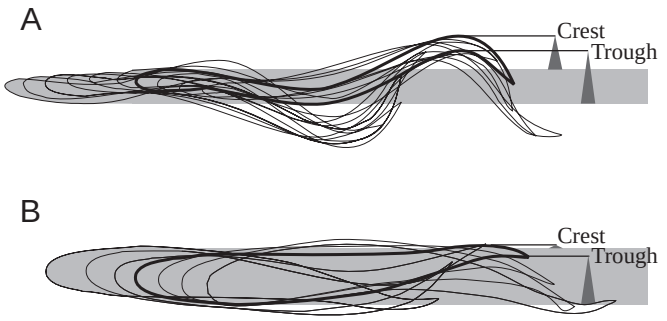

Fig. 8. Body contours over one tail-beat of (A) an eel and (B) a mullet swimming steadily at $1.4\,L\,s^{-1}$ (slip 0.6–0.7, where L is body length). The time between contours is 0.04 s. The light-shaded area indicates the initial water displacement by the head. The maximum crests (thick black line) of the body wave extend considerably beyond this initial displacement only in the eel (grey triangles). This means that only the eel generates strong high-pressure flows. The troughs (thick black line) recess significantly beyond the initial displacement of the head in both fish (grey triangles). This causes strong low-pressure flows in both species.

et al., 2000) predict strong transverse flows out of the mediofrontal plane near the nodes of the body wave and predominantly longitudinal flows where the body wave reaches a lateral maximum. From our two-dimensional flow fields, we can calculate divergence (Stamhuis and Videler, 1995) to estimate the absence or presence of out-of-plane flows in incompressible fluids. We observe weak divergence at the head and slightly higher values in the tail region. The caudal out-of-plane flows concentrate in the areas of high flow velocity between the node and the lateral extreme of the body wave.

Eels generate more pronounced longitudinal flows than the previously studied fusiform swimmers for several reasons. First, they have a larger body wave amplitude and a shorter body wave length. Both aspects can contribute to higher lateral body velocities. Second, bodies of almost uniform width displace water in a different way from strongly tapered fusiform bodies. In a fusiform body, the lateral excursion of the body at the crest of a body wave does not significantly exceed the initial displacement of water at the head. Noticeable crests develop only in the peduncle region (Fig. 8A). Hence, for fusiform undulating bodies, the water displacement and the momentum transfer are largest at the troughs and only weak at the crests (Müller et al., 1997; Wolfgang et al., 1999). Slender fish such as eels generate substantial lateral movement beyond the initial head displacement along the entire body (Fig. 8B). Hence, significant pressure gradients build up in the crests as well as the troughs of the body wave.

These flows along the body contain the momentum transferred to the water by the body, but they cannot be equated with the body's contribution to thrust production and simply be added to the tail's thrust output: the body flows interact with the tail flows and modify the tail's performance.

Wake generation in undulatory swimmers

As the body flows reach the tail, they cause the shedding of a body vortex off the trailing edge of the tail tip. Independently from the shedding of this body-generated vortex, start–stop vortices are shed off the tail every time the tail reaches a lateral extreme and changes direction. The phase between body and tail movements determines whether consecutive body and tail vortices are shed separately, as in our eel, or merge into one vortex, as in our previous experiments with mullet (Müller et al., 1997). This sensitivity of the wake shape to the phase relationship between two vortex generators was established by Gopalkrishnan et al. (Gopalkrishnan et al., 1994) and Streitlien et al. (Streitlien et al., 1996), including its relevance for maximising thrust or efficiency.

In the case of our eel, the 'proto-vortex' travels down the body. It crosses the mean path of motion before it is shed as a body vortex off the tail tip on the contralateral side of where it was first observed. We observe the following shedding pattern in the mediofrontal cross section of the wake. The body sheds a single row of alternating vortices close to the mean path of motion. These lie inside a reverse von Kármán vortex street shed by the tail. Consecutive body and tail vortices counter-rotate and form one vortex pair per half tail-beat cycle. The circulations of the body and the tail vortex are similar immediately after shedding, indicating that body vortices contribute equally to the wake and probably to thrust. In previous studies on mullet (Müller et al., 1997) and danios (Wolfgang et al., 1999), the body vortex is shed together with a tail vortex of the same rotational sense. Body and tail vortices combine into a single vortex. The resulting cross section through the wake consists of a reverse von Kármán vortex street with two single rows of counter-rotating vortices.

Wake morphology is the result of the interaction between the circulation building up around the tail and the momentum generated by the undulatory pump action of the body. This interaction depends on the phase relationship between the tail-beat cycle and the body wave travelling down the body. It can be shown analytically (see Appendix) that a non-uniform amplitude envelope causes a phase shift between the lateral displacement function of the body and the pressure difference across the midplane of the fish. Assuming a constant body wave length, the phase shift causes the 'proto-vortex' to be shed off the tail not on the mean path of motion, but offset laterally. A phase shift can be the result either solely of a non-uniform amplitude envelope or of the interaction between the former and a changing body wave length along the body. The sensitivity of the phase relationship to slight changes in the amplitude envelope and the wave length might explain how undulatory swimmers can produce wakes with single vortices and vortex pairs at similar U/V ratios. Eel-type swimmers can adapt their kinematics to produce a double (Hertel, 1966; Rayner, 1995; present study) or single (Gray, 1968) vortex wake. Saithe-type swimmers have been reported to produce vortex-pair wakes (Rosen, 1959) as well as single-vortex wakes (Aleyev, 1977; Blickhan et al., 1992; Müller et al., 1997; Wolfgang et al., 1999).

Some data exist in the literature mapping the phase between lateral displacement function and body curvature, and several

studies did indeed find a variety of phase relationships in several undulatory swimmers (Gillis, 1997; Jayne and Lauder, 1995; Katz and Shadwick, 1998; Müller et al., 1997; Videler and Hess, 1984). These experimental data on the variable phase within body wave parameters – such as node and inflection point – make it likely that a similar variability exists between these body wave parameters and the body-generated flow patterns. However, the experimental evidence for a correlation between body wave parameters and body vortex shedding is far from conclusive. Data on the relationship between vortex shedding and body kinematics are still very sparse (Müller et al., 1997; Wolfgang et al., 1999).

Experimental and theoretical approaches alike suggest that fish might change their body wave to cause changes in the phase relationship between body and tail movements, which in turn affect the phase between body and tail flow. The result is a fine control over the interaction between body and tail vortices and the vortex shedding pattern that reflects the optimisation criteria employed by the fish at each moment. The range of flow patterns observed behind undulatory swimmers to date can be explained in terms of the proposed control over body and tail vorticity. The wake of an undulatory swimmer will be a strong reverse von Kármán vortex street only if the fish is maximising thrust. When maximising efficiency, the resulting wake is a weak reverse von Kármán vortex street, which can verge on a drag wake depending on the relative strength of the merging counter-rotating body and tail vortices. Maximising thrust or efficiency requires a specific phase relationship between body and tail vortex shedding. For a phase relationship midway between the two optima, yet another wake pattern is generated. This is the vortex-pair wake observed in the present study.

Concluding remarks

The morphology of the wake and the flow adjacent to the eel's body support the hypothesis that the eel employs its whole body to generate thrust. The maximum flow velocities adjacent to the body increase approximately linearly from head to tail. The tail-beat kinematics is only one factor besides the body wave that determines the shape of the wake. The shape of the wake deviates strongly from an optimised wake for maximising hydrodynamic efficiency or thrust, as suggested by Triantafyllou et al. (Triantafyllou et al., 1991; Triantafyllou et al., 1993) and observed in mullet (Müller et al., 1997) and trout (Blickhan et al., 1992). Instead, it resembles the flow pattern described by Gopalkrishnan et al. (Gopalkrishnan et al.1994) for a phase relationship between maximum thrust and efficiency, where neither is particularly high.

Appendix

Lighthill's small-amplitude slender body theory (Lighthill, 1960) can be used to derive a qualitative estimate for the phase relationship between 'proto-vortex' and body wave parameters. Lighthill's model describes the pressure distribution across the body. We assume that the centre of a 'proto-vortex' lies at the point where the pressure difference DW across the fish is zero. This approach neglects the effects of the wake on the pressure distribution on the body, the details of the shedding process and added-mass effects. We compare pressure distribution and body wave, in particular the positions of nodes and inflection points, for two simple amplitude envelopes. The analysed body wave geometries neglect the existence of a pivot point and assume a constant body wave length. We also assume that the cross-sectional area A of the eel's body is constant. The main objective of this comparison is to see whether the 'proto-vortex' will be shed on the mean path of motion (node and vortex centre coincide at the tail tip) and whether it coincides with the inflection point at the moment of shedding.

Let the midline displacement, relative to the mean path of motion x, be $h(t,x)$ and the lateral velocity of the midline $V(t,x)$ be:

$$V(t,x) = \left(\frac{\partial h}{\partial t} + U\frac{\partial h}{\partial x}\right), \tag{A1}$$

where U is the swimming speed. Then, according to Lighthill (Lighthill, 1960), the instantaneous lift per unit length of fish $F_L(t,x)$ is:

$$F_L = -\rho\left(\frac{\partial}{\partial t} + U\frac{\partial}{\partial x}\right)\left(\frac{\partial h}{\partial t} + U\frac{\partial h}{\partial x}\right)A\,. \tag{A2}$$

With A and the density of water ρ being constant along the body, the pressure difference DW across the body is proportional to:

$$DW \propto \left(\frac{\partial}{\partial t} + U\frac{\partial}{\partial x}\right)\left(\frac{\partial h}{\partial t} + U\frac{\partial h}{\partial x}\right). \tag{A3}$$

The centre of the 'proto-vortex' should be at DW=0. The inflection point is where $\partial^2 h/\partial x^2$=0 and the node is at h=0. Now consider two cases.

Uniform amplitude envelope

h=$A\cos k(x–Vt)$, where V is the wave speed and k is the wave number. Then

$$\frac{\partial^2 h}{\partial x^2} = -k^2 A\cos\theta\,, \tag{A4}$$

where θ=$k(x–Vt)$ and DW=$–k^2A(V–U)^2\cos\theta$. In this case, DW=0, and node and inflection point coincide. All reach the tail when h=0.

Linearly increasing amplitude envelope

h=$A(x/L)\cos k(x–Vt)$, where L is the body length of the fish. Then:

$$\frac{\partial^2 h}{\partial x^2} = -A\frac{x}{L}k^2\cos\theta - 2A\frac{k}{L}\sin\theta\,, \tag{A5}$$

while

$$DW = -Ak^2\frac{x}{L}(V-U)^2\cos\theta + 2A\frac{k}{L}U(V-U)\sin\theta\,. \tag{A6}$$

Therefore, $\partial^2h/\partial x^2=0$ where $\tan\theta=-kx/2$, while $DW=0$ where $\tan\theta=+kx/2(V/U-1)$. Note that, in this case, $\partial^2h/\partial x^2=0$ at $x=L=0$ when $\tan\theta=1/kL$, and $h=0$ at $x=L$ when $\cos\theta=0$, which is not necessarily at the same time as the 'proto-vortex' reaches the tail tip, depending on the values of kL and V/U. Hence, node, inflection point and vortex centre do not necessarily coincide, and the vortex is shed at the tail tip not on the mean path of motion but offset laterally.

We would like to thank The Eelfarm in Bedum, the Netherlands, for providing the eels and BASF for providing the polystyrene particles. Tim Pedley helped iron out inconsistencies in the hydrodynamic interpretation of the data, in particular in the Appendix. Michael Dickinson and an anonymous referee are gratefully acknowledged for their helpful suggestions. This research was conducted by U.K.M. as part of a PhD under the supervision of J.J.V. and funded by the University of Groningen. J.S. and Maaike Binner recorded the flow fields presented here as part of MSc projects under the supervision of U.K.M.. E.J.S. wrote most of the flow-analysis software and designed the image-recording system.

References

Aleyev, Y. G. (1977). *Nekton*. The Hague: Dr. W. Junk. 435pp.

Blickhan, R., Krick, C., Zehren, D. and Nachtigall, W. (1992). Generation of a vortex chain in the wake of a subundulatory swimmer. *Naturwissenschaften* **79**, 220–221.

Carling, J., Williams, T. L. and Bowtell, G. (1998). Self-propelled anguilliform swimming: simultaneous solution of the two-dimensional Navier–Stokes equations and Newton's laws of motion. *J. Exp. Biol.* **201**, 3143–3166.

Chen, C. J., Kim, Y. G. and Walter, J. A. (1993). Progress in quantitative flow visualisation and imaging process. In *Atlas of Visualisation* (ed. The Visualization Society of Japan), pp. 279–296. Oxford: Pergamon Press.

Gillis, G. B. (1997). Anguilliform locomotion in an elongate salamander (*Siren intermedia*): effects of speed on axial undulatory movements. *J. Exp. Biol*. **200**, 767–784.

Gopalkrishnan, R., Triantafyllou, M. S., Triantafyllou, G. S. and Barrett, D. S. (1994). Active vorticity control in a shear flow using a flapping foil. *J. Fluid Mech.* **274**, 1–21.

Gray, J. (1968). *Animal Locomotion*. London: Weidenfeld & Nicolson. 479pp.

Hertel, H. (1966). *Structure, Form, Movement*. New York: Reinhold Publishing Corp. 251pp.

Hess, F. (1983). Bending movements and muscle power in swimming fish. *Proceedings of the Australian Fluid Mechanics Conference*, vol. 2, pp. 12A1–12A3. University of Newcastle, New South Wales.

Jayne, B. C. and Lauder, G. V. (1995). Speed effects on midline kinematics during steady undulatory swimming of largemouth bass, *Micropterus salmoides*. *J. Exp. Biol.* **198**, 585–602.

Katz, S. L. and Shadwick, R. E. (1998). Curvature of swimming fish midlines as an index of muscle strain suggests swimming muscle produces net positive work. *J. Theor. Biol.* **193**, 243–256.

Keane, R. D. and Adrian, R. J. (1991). Optimization of particle image velocimeters. Part II. Multiple pulsed systems. *Measurement Sci. Tech.* **2**, 963–974.

Lighthill, M. J. (1960). Note on the swimming of slender fish. *J. Fluid Mech.* **9**, 305–317.

Lighthill, M. J. (1969). Hydrodynamics of aquatic animal propulsion. *Annu. Rev. Fluid Mech.* **1**, 413–446.

Merzkirch, W. (1987). *Flow Visualisation*. Second edition. Orlando: Academic Press. 260pp.

Müller, U. K., van den Heuvel, B. L. E., Stamhuis, E. J. and Videler, J. J. (1997). Fish foot prints: morphology and energetics of the wake behind a continuously swimming mullet (*Chelon labrosus*). *J. Exp. Biol.* **200**, 2893–2906.

Pedley, T. J. and Hill, S. J. (1999). Large-amplitude undulatory fish swimming: fluid mechanics coupled to internal mechanics. *J. Exp. Biol.* **202**, 3431–3438.

Rayner, J. M. V. (1985). Vorticity and propulsion mechanics in swimming and flying vertebrates. In *Konstruktionsprinzipien Lebender und Ausgestorbener Reptilien* (ed. J. Riess and E. Frey), pp. 89–118. Universities of Stuttgart and Tübingen: Konzepte SFB 230, 4.

Rayner, J. M. V. (1995). Dynamics of the vortex wakes of flying and swimming vertebrates. In *Biological Fluid Dynamics* (ed. C. P. Ellington and T. J. Pedley), pp. 131–155. Cambridge: Company of Biologist Ltd.

Rosen, M. W. (1959). *Water Flow about a Swimming Fish*. China Lake, CA: U.S. Naval Ordnance Test Station TP 2298. 96pp.

Spedding, G. R., Rayner, J. M. V. and Pennycuick, C. J. (1984). Momentum and energy in the wake of a pigeon (*Columbia livia*) in slow flight. *J. Exp. Biol.* **111**, 81–102.

Stamhuis, E. J. and Videler, J. J. (1995). Quantitative flow analysis around aquatic animals using laser sheet particle image velocimetry. *J. Exp. Biol.* **198**, 283–294.

Streitlien, K., Triantafyllou, G. S. and Triantafyllou, M. S. (1996). Efficient foil propulsion through vortex control. *AIAA J.* **34**, 2315–2319.

Triantafyllou, M. S., Triantafyllou, G. S. and Gopalkrishnan, R. (1991). Wake mechanics for thrust generation in oscillating foils. *Phys. Fluids* A **3**, 2835–2837.

Triantafyllou, M. S., Triantafyllou, G. S. and Grosenbaugh, M. A. (1993). Optimal thrust development in oscillating foils with application to fish propulsion. *J. Fluid Struct.* **7**, 205–224.

Triantafyllou, M. S., Triantafyllou, G. S. and Yue, D. K. P. (2000). Hydrodynamics of fishlike swimming. *Annu. Rev. Fluid Mech.* **32**, 33–53.

Videler, J. J. (1993). *Fish Swimming*. London: Chapman & Hall, 260pp.

Videler, J. J. and Hess, F. (1984). Fast continuous swimming of two pelagic predators, saithe (*Pollachius virens*) and mackerel (*Scomber scombrus*): a kinematic analysis. *J. Exp. Biol.* **109**, 209–228.

Videler, J. J., Müller, U. K. and Stamhuis, E. J. (1999). Aquatic vertebrate locomotion: wakes from body waves. *J. Exp. Biol*. **202**, 3423–3430.

Vollmers, H., Kreplin, H.-P. and Meier, H. U. (1983). Separation and vortical-type flow around a prolate spheroid – evaluation of relevant parameters. *NATO AGARD Conference Proceedings No.* **342**, pp. 14/1–14/14.

Wolfgang, M. J., Anderson, J. M., Grosenbaugh, M. A., Yue, D. K. P. and Triantafyllou, M. S. (1999). Near-body flow dynamics in swimming fish. *J. Exp. Biol.* **202**, 2303–2327.